Rock Mechanics and Rock Engineering (2019) 52:1903–1916
https://doi.org/10.1007/s00603-018-1716-6

ORIGINAL PAPER

Mining-Induced Deformation in the Malmberget Mine

Tristan Jones[1,3] · Erling Nordlund[1] · Thomas Wettainen[2]

Received: 18 April 2018 / Accepted: 14 December 2018 / Published online: 7 January 2019

Abstract
The Norra Alliansen orebody of the Malmberget sublevel caving mine consists of iron ore interspersed with biotite schist and granitic inclusions. The schist is squeezed between the ore and the host rock and in direct contact with the ore along the majority of the length of the footwall. The schist exhibits high deformation when exposed to stress. SMART cable bolt roof deformation measurements are re-analyzed to draw conclusions regarding the patterns of deformation in the mine. Each bolt's head is placed at the origin of a spherical coordinate system and the radius and inclination angle between the bolt and every production blast occurring during the bolt's recorded lifetime are calculated. The deformation experienced by each instrument is investigated by comparing the long-term recorded movements with the developed geometric variables. Patterns of deformation magnitude and rate are found with respect to production-blast distance and inclination angle, instrument location, rock quality designation, and likely mining-induced stresses. Results show that deformation magnitude tends to be higher when driven by production blasting occurring on the production level above the instrumentation when accounting for the effects of distance, but average deformation magnitude for very-near production blasts tends to be higher than that for production blasts occurring directly above the instrument. Correlations also exist between the measured RQD, estimated rockmass parameters, and the measured deformation. Empirical evidence allows the identification of six scenarios which account for 91% of the recorded high-deformation-rate events. These scenarios help determine which production activities are most likely to cause high deformation rates.

Keywords Roof deformation · Mining-induced deformation · Sublevel caving · Instrumented bolts · Mining · Ground control

1 Introduction

1.1 Empirical Research in Mining

Empirical research in bulk extraction (caving and open stoping) mining methods has tended towards improvements in efficiency or mine design. Prior empirical investigations have focused on ore dilution, draw control, stability, or safe and efficient caving initiation (Matthews et al. 1980; Pakalnis 1986; Rech and Watson 1994; Swart and Handley 2005; Capes et al. 2007; Brunton et al. 2010; Jin et al. 2017). Surface subsidence, which lends itself well to empirical research due to the ease of accessibility and availability of various measurement methods, has also been extensively researched empirically (Lupo 1996; Henry et al. 2004; Villegas et al. 2011; Chen et al. 2013; Woo et al. 2013; Wettainen and Martinsson 2014).

The references above are intended to illustrate that while empirical research has been used extensively within the bulk extraction methods, those topics which have benefitted most and received the greatest attention have been highly production- and subsidence-focused. Those studies that have been completed with respect to underground entry deformation and stability have been location-specific. Mining-induced entry deformation has been approached indirectly

✉ Tristan Jones
tristan.jones@lkab.com

Erling Nordlund
erling.nordlund@ltu.se

Thomas Wettainen
thomas.wettainen@lkab.com

[1] Division of Mining and Geotechnical Engineering, Luleå University of Technology, 971 87 Luleå, Sweden

[2] Luossavaara-Kiirunavaara AB (publ), 983 81 Malmberget, Sweden

[3] Present Address: Luossavaara-Kiirunavaara AB (publ), 983 81 Malmberget, Sweden

(Blanchowski et al. 2011), though that study utilized surface-based GPS measurements to indirectly determine rockmass deformation via numerical modeling. It has also been used to identify the occurrence of shear failure or bending in the footwall or hangingwall (Hidalgo and Nordlund 2014).

Empirical research has been useful for the prediction and control of entry convergence and deformation underground. It has been noted that rock mass strength is often correlated with convergence, weaker zones being affected more than stronger zones and that it can be critical for estimation of cumulative closure (Struthers et al. 2000). The same study noted that closure rates were related to stress levels and rock mass quality and that deformation changes could be seen as the abutment stresses from the level above move across the level. While this experience has many similarities to the current efforts, it focuses on the redesign of the sublevel caving levels to allow for successful mining, and on predictions of closure rate to determine estimated entry lifespan.

The Argyle mine has successfully used damage mapping, geotechnical indexing and convergence measurements to develop a cumulative convergence model for its operation (Fernandez et al. 2012). The primary outcome was a predictive nomogram that utilizes rock quality geologic strength index (GSI) and distance to the undercutting front to determine expected convergence. As Argyle is a block caving operation, it tends to have a gradually moving caving front, dissimilar from a sublevel caving operation, which tends to have more sudden changes in the local stress fields corresponding to individual production blasts.

One of the most systematic applications of empirical design to improve entry conditions has occurred in the underground coal industry, which has developed many tools utilizing simple relationships to better understand geotechnical phenomena. Stress and strain measurements have been part of this effort, but deformation within and at the surface of the rock mass has been a significant addition used to help better understand the geotechnical challenges. Some critical advances in coal mine ground control have been simply due to the identification of empirical relationships between the relative position of the mining face and the stresses or deformation measured at a location of interest (Wagner 1974; Dahl 1978; Salamon and Wagner 1985; Mark 1987; Bieniawski 1992; Mark and Chase 1997; Colwell et al. 2003; Colwell 2006).

The focus of this paper is on how specific production scenarios can combine with geologic and rock mechanical parameters in a location to affect deformation. It uses deformation measurements to monitor changes in the rock following production blasting. Initially the paper considers general deformation trends and relates them to the 3D position of production blasting relative to the location of the instrumentation. It then considers the impact of specific production activities to better understand how these independent events affect deformation in the immediate sense. Examples of such activities include the opening blasts of a new crosscut or when production blasting occurs directly over an instrument on the level above. Better understanding of these effects should allow for better production sequencing, minimization of deformation, and reduced risk to employees and production.

This study takes a new look at an older dataset (Sundström 2010) and uses it to examine the impact of production blasts and the mining-induced deformation they produce. While the main goal of Sundström's work was to determine if deformation measurements could be used to identify a deformation threshold indicating the need for the installation of additional support elements, this paper aims to better understand which production activities produce different deformation trends in the mine. Changes in deformation were measured by a suite of instrumented cable bolts, with deformation and deformation rate being the primary dependent variables. The deformations, presumably caused by stress redistribution, vary greatly depending on the geology and the relative position of the blasts with respect to the instrumented locations.

1.2 Study Site

Sweden's LKAB mining company was founded in 1890, though mining in the region goes back to 1660s when the first iron ore sample was collected. The Malmberget sublevel caving mine comprises some 20 orebodies, of which about half of them are in production today. It is in the Gällivare municipality, Norrbotten county, in northern Sweden. Today's mining is between 800 and 1200-m depth and distributed over an area approximately 2.5 km × 5 km in size (NS × EW). The orebody dip varies between 45° and 75°, with an average dip of 45°–50°.

The Norra Alliansen orebody is one of the largest in the mine. It strikes east to west, dips 60° to the south, has an average width of around 50 m, and daylights at the surface. The ore field is strongly affected by regional metamorphosis and is hosted in volcanite host rocks called leptites, which range in color from gray through red-gray and red, with increasing strength. The ore consists of magnetite with smaller amounts of hematite and contains several ore lenses and granitic dikes. Biotite schist is common, existing especially along the footwall contact zone between the ore and the leptites. Alliansen orebody merges with the Printzsköld orebody at around 1000 m depth, resulting in a 2-km long orebody.

Sublevel caving production in Norra Alliansen occurs by developing a series of footwall drifts and perpendicular crosscuts undercutting the ore. Each crosscut is divided into a series of blast rings, each consisting of 8–14 production holes drilled from the roof of the crosscut up into the ore.

When these rings are blasted it fractures the ore allowing it to cave. The ore is removed via loader and taken for further processing. The blasting, caving and removal of the ore causes a great deal of stress redistribution and accompanying deformation nearby. Blasting occurs on multiple sublevels at the same time.

At the time of data collection, general ground support in the mine consisted of 30–50-mm unreinforced shotcrete applied during development. Each development blast also included two rings of 3-m long rock bolts with center-to-center spacings of 2.0–2.5 m. In more difficult conditions, such as those in the study areas, bolt spacing was reduced and 80–100 mm of fiber-reinforced shotcrete was applied. The same support was used in all study areas.

2 Instrumentation and Data

2.1 Deformation Data

Between May, 2007 and April, 2010 deformation data was acquired from a suite of 20 SMART (Stress Measurement to Assess Reinforcement Tension) cable bolts installed on levels 932 and 962 of the Norra Alliansen orebody (Fig. 1) (Sundström 2010). The SMART cable bolt is a standard 7-strand cable bolt mixed with a miniature 6-wire extensometer with a 63.5-mm stroke length and a linearity of ±2% (Mine Design Technologies 2018). The instrument and data reader had a combined accuracy of 0.127 ± 0.003 mm. Five pairs of bolts were installed on each level and grouped so that comparisons could be made between similar geologies. A description of the groups and instrument locations is found in Table 1.

Bolts 1–10 operated from May, 2007 until November, 2007 on level 932, and bolts 11–20 from July, 2007 until April, 2010 on level 962. Bolts were installed vertically in the center of the crosscut roof, with anchors at the collar (0.00-m), 0.50-m, 1.00-m, 1.50-m, 2.00-m, 3.00-m and 5.00-m depths. Data were acquired manually, averaging once every 4.6 days over the same period, though the time between readings was significantly longer in some instances. The independent variables were the distance (r) and inclination angle (φ) between each individual instrument and the location of each production blast, which occurred once every 2.4 days on average. To directly compare independent and dependent variables, average-weekly deformation, average-weekly deformation rate, average-weekly distance, and average-weekly inclination were used for much of the

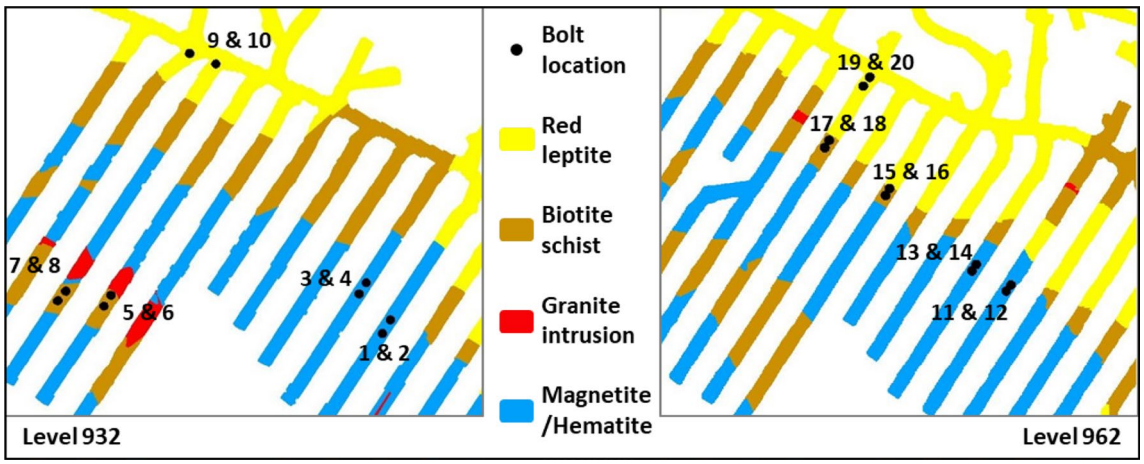

Fig. 1 Geologic map showing levels 932 and 962, with installed instrument locations

Table 1 Bolt identification and description of instrument installation locations

Bolt ID's (group)	Geology	Installation notes and description
1–4, 11–14 (A)	Magnetite ore	Competent and stiff. Preferentially accepts load from the weaker host rock. Full extraction occurs on the level above
5–8 (B)	Biotite schist near granite intrusion	Weak, low-stiffness rock between two parts of orebody, contacts intrusion. Full extraction occurs on the level above
9, 10, 19, 20 (C)	Red leptite footwall	High-quality, high-stiffness host rock with minimal extraction directly above
15–18 (D)	Biotite schist, footwall contact	Weak, low-stiffness host rock. Full extraction occurs on the level above

analysis (Sundström 2010; Jones 2016). A full explanation is offered in the next section.

Roof deformation relative to the toe-anchor of the extensometer was used, and deformation rate was calculated by simply dividing the amount of deformation that had occurred since the previous measurement by the number of days between measurements. This produced an average daily deformation rate. Deformation is greatest at the collar, which represents the greatest hazard for falling material and instability. Other anchors were used for interpretation. Deformation and deformation rate were the dependent variables used in the study. Load values were also calculated from the deformation data and were used to estimate when the bolt passed beyond its elastic range.

2.2 Instrument to Production-Blast Vectors

The absolute location of each instrumented bolt head (the instrument location) was identified by its *XYZ* coordinates within a global mine coordinate system, as determined from mine maps and survey locations. The *XYZ* location of each production blast was also determined within the same coordinate system. For this study the blast location was defined as the point on the centerline of the crosscut floor, directly beneath the blast ring for that blast. The burden for each blast was 3.5 m, only differing for the opening three rings in each crosscut which were spaced 1.2 m apart. In total, 1015 production blast rings were detonated in Alliansen during the instrumented time period, averaging one blast every 2.4 days, though this included instances where the time between blasts was much greater than this average (Sundström 2010; Jones 2016).

Once all instruments and blasts were located, vectors were developed originating from every instrument location, extending to the location of each production blast that occurred during that instrument's data record. Since not every instrument was operational for every production blast, there was a total of 12,123 reliable vectors. The components of the vectors were the independent variables.

A spherical coordinate system was used to describe the vectors (Fig. 2), such that of the vector components included:

- length (radius, r), corresponding to the distance on the horizontal plane between the instrument and the blast in question,
- azimuth (θ), the direction of the blast in degrees (± 180), with zero degrees aligned with local mine north,
- inclination angle (φ), the angle in degrees above or below the horizontal plane (Fig. 2).

Setting each instrument at the origin of its own coordinate system allowed analysis to be done individually to identify specific factors contributing to deformation for individual bolts, yet all the results could be collated and analyzed cumulatively to investigate mine-wide or group-wide trends. Since the manual instrument readings did not occur at the exact same time as each of the production blasts, independent variables were also averaged on a weekly basis, as with the deformation data.

2.3 Strength and Rock-Quality Parameters

Geologic strength data was acquired from previous research completed in the vicinity and from communication with the mine (Table 2). Most of the rock units are relatively straightforward, but the biotite schist can have highly-variable properties. While technically only one biotite schist unit exists, previous publications have tended to subdivide

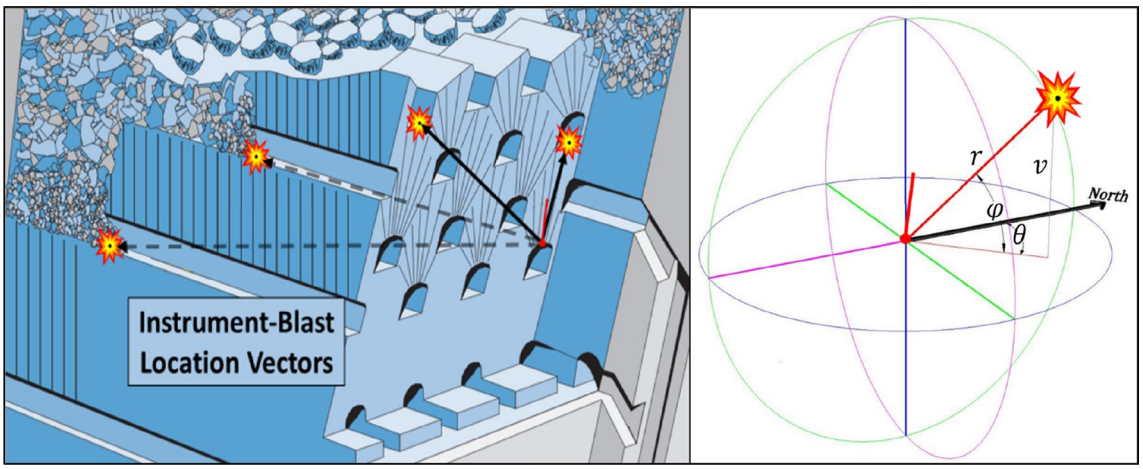

Fig. 2 Isometric view of Blast-Instrument vectors (left) and depiction of the spherical coordinate system used to define relative positioning (right). Isometric drawing adapted from Atlas Copco (2007)

Table 2 Geotechnical parameters of common Malmberget rocks including uniaxial compressive/tensile strength (UCS/UTS), GSI and rock mass rating (RMR)

Rock type	UCS[a] (MPa)	UCS[b] (MPa)	GSI[a]	UTS[a] (MPa)	UTS[b] (MPa)	RMR[b]	Ore contact distance (m)[b]	Thickness (m)[b]
Magnetite	100 ± 8		55–65	5.0				
Biotite schist 1	40–60	5–30	35–45		0–5	35	0.5–5	0.5–5
Biotite schist 2	90–100	30–50	45–55		5–10	40	5–20	5–10
Biotite schist 3	N/A	50–80	N/A	N/A	10–20	45	20–50	20–30
Grey leptite	80 ± 8		60–70	8.5 ± 0.7				
Red-grey leptite	176 ± 60		65–75	11 ± 2.8				
Red leptite	217 ± 50		65–75	14.5 ± 3.5				

[a]Basarir (2013), Idris et al. (2013)

[b]Nordlund (2013)

it into two (Basarir 2013; Idris et al. 2013) or three (Nordlund 2013) domains for geotechnical-modeling purposes. The strength of the domains varies considerably, the weakest being adjacent to the ore (Basarir 2013; Idris et al. 2013; Nordlund 2013). It is the weakest of all geologic units commonly encountered in the mine and frequently requires supplementary support as it deforms and falls more than the rocks around it. Strength and RMR values helped interpret the instrument results.

3 Production-Blast Location and Deformation

3.1 Distance-Based Relationships

All of the bolts installed in magnetite or red leptite (groups A and C) recorded nearly zero deformation regardless of the independent variables. This strongly indicates that the support regime installed in these areas was adequate given the rock quality in these locations (Table 2). Alternately, the bolts from Groups B and D were all installed in the biotite schist which had a lower rock quality. These areas had the same rock support as that installed for groups A and C, but the bolts showed clear deformation. Figures 3, 4 and 5 show the deformation magnitude with respect to production-blast distance (r). The distance between each blast and instrument location (as defined in Sect. 2.2) is plotted on the left axis according to colors indicating the production level on which the blast occurred, and average-weekly distance is shown. These can be compared with the recorded displacement from each of the SMART bolts plotted on the right axis.

The initial data point for all bolts was collected on the 9th of May, 2007 (day 1), 24 h after the installation of all bolts. Table 3 provides detailed information about the lifespan, instrumentation location, and the location of and distance to the final blast recorded from within that instrument's crosscut.

Most instruments stopped functioning either because blasting occurred close enough for a blast's dynamic pulse to destroy the instrument, or because of general rock mass failure. However, bolts 17 and 18 (Fig. 6) experienced enough deformation that their potentiometers over-ranged and ceased recording before blasting in their crosscuts was close. They were located approximately 130 m and 33 m, respectively, from the brow when they ceased recording. Their load records indicated that bolt 17 entered its plastic range on day 386, while bolt 18 did so on day 544, the same time as general production ceased on level 932. No other bolts experienced plastic deformation during their measurement.

Much of the differences in deformation recorded on different instruments can be attributed to the differences in rock type, with the biotite schist having natural laminations and anisotropic shear tendencies, while the granite leptites are naturally stronger and less deformable. In addition to this, the biotite schist generally has a higher number of joints occurring within upon which sliding and deformation can occur (Sundström 2010). In the original 2010 study, location-specific RQD was determined from observation cores in the instrumented areas (Sundström 2010). These results are presented in Table 4. Site-specific RMR or GSI values cannot be determined from available data about the study locations, but generalized rockmass values for the same geology on lower levels of the mine have been added to Table 4 for reference purposes. Correlations exist between the measured RQD, estimated rockmass parameters, and the measured deformation. These types of relationship are reasonable given the relationship between the moduli of elasticity and deformation (Coon and Merritt 1970; Franklin and Dusseault 1989; Deere et al. 1996).

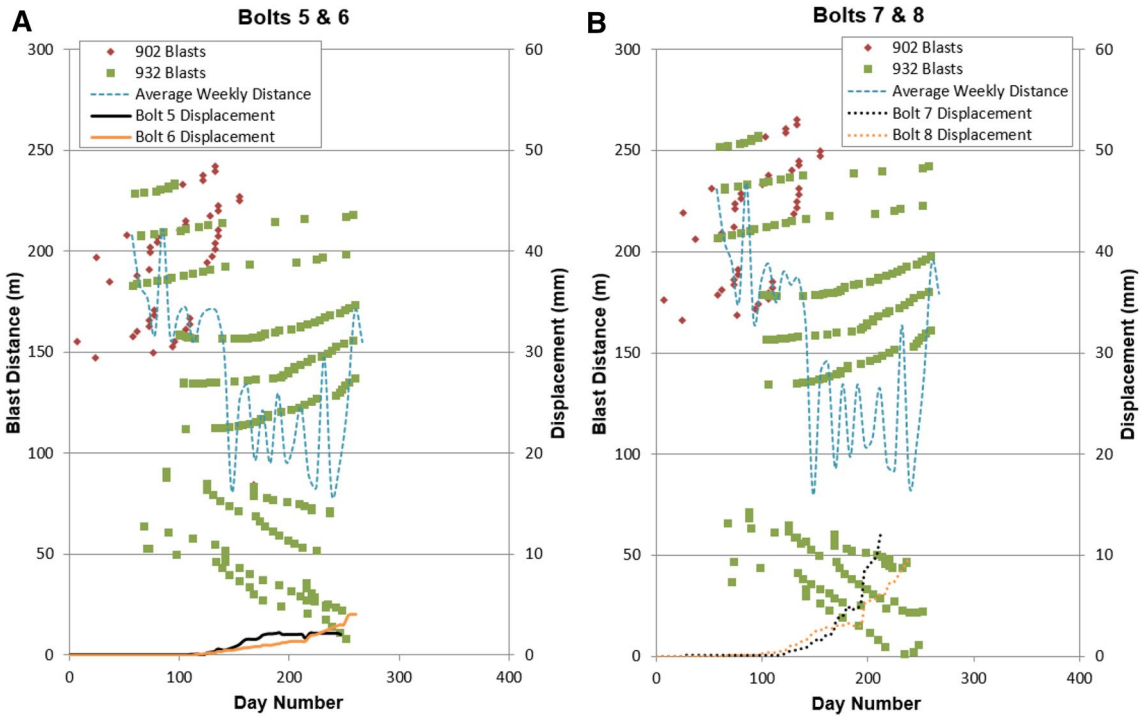

Fig. 3 Graphs showing the deformation magnitude of bolts 5 and 6 (**a**) and 7 and 8 (**b**) on level 932 m relative to production-blast distance

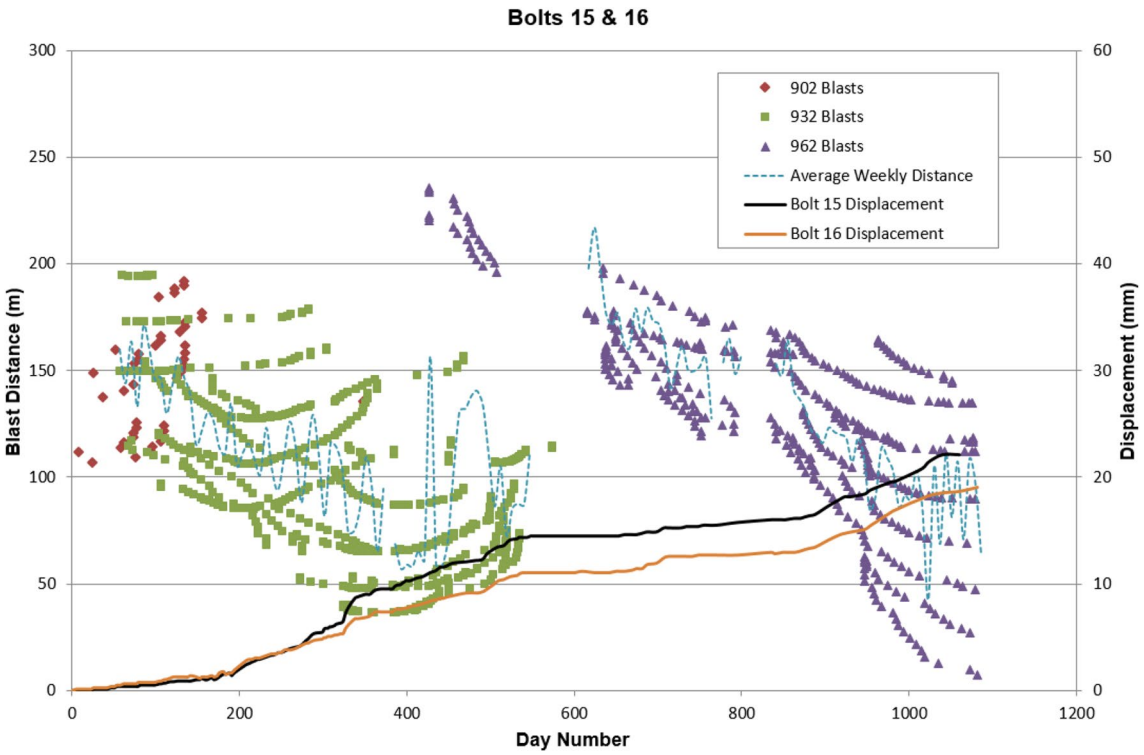

Fig. 4 Graphs showing the deformation magnitude of bolts 15 and 16 on level 962 m relative to production-blast distance

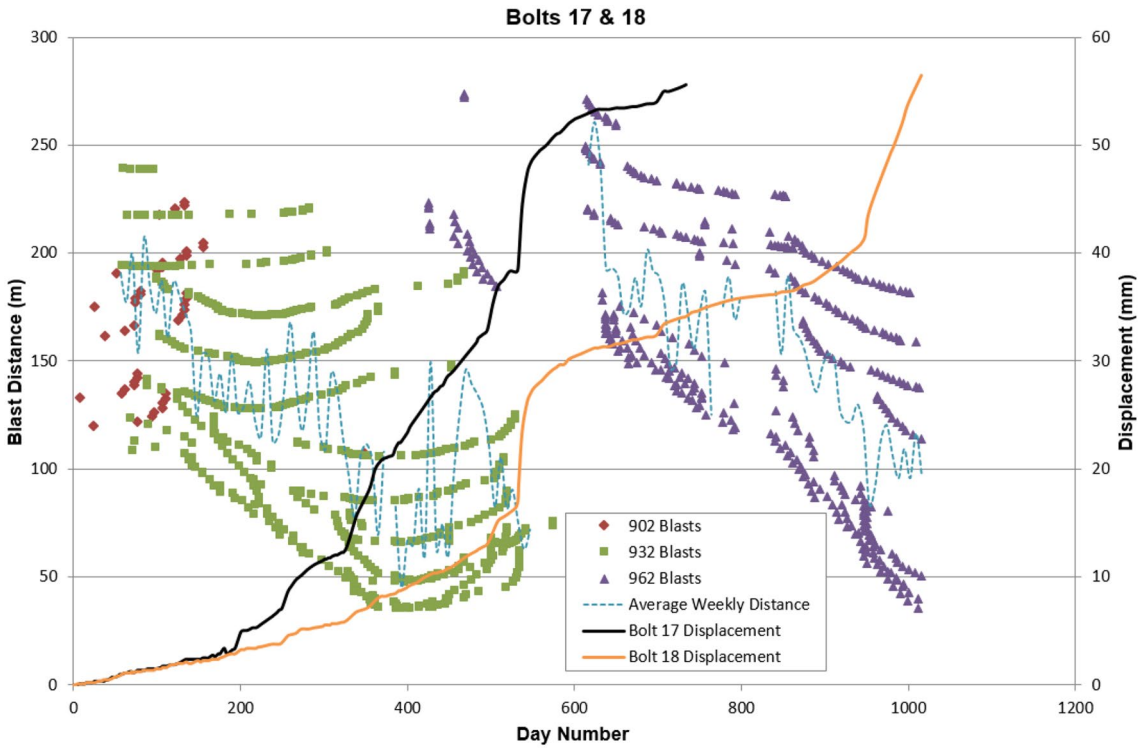

Fig. 5 Graphs showing the deformation magnitude of bolts 17 and 18 on level 962 m relative to production-blast distance

Table 3 Timing and distance data showing the day on which the final instrument record was made, the day of the last production blast recorded by that instrument, the ring in which the instrument was installed, and the ring of the last blast. Also, the distance between the instrument and the final recorded blast

Bolt #	Last-recorded blast day	Final bolt record day	Instal-lation ring	Final blast ring	Final blast distance (m)
5	239	247	19	18	2
6	252	261	22	21	2
7	210	215	17	16	2
8	235	240	19	18	3
15	1035	1060	21	19	8
16	1081	1081	23	21	3
17	729	734	47	11	130
18	1012	1016	49	40	33

3.2 Inclination Angle-Based Relationships

Inclination angle (φ—as defined in Sect. 2.2) provides useful insight into the patterns of deformation. As can be seen in Fig. 2, φ and r are directly linked to one another trigonometrically according to:

$$\sin\varphi = \frac{v}{r}$$

where (r) is determined from the instrument-production blast vectors and becomes the hypotenuse of a right triangle determined by the vertical separation (v) between the blast location and the instrument location. The distance-based element of deformation must be accounted for to see inclination angle's impact.

By dividing r into 10-m long distance-ranges, or "bins", a histogram showing the average-weekly deformation rate that occurred in each range allows direct comparison between same-level and the level-above blasts. In every distance-range in which blasting occurred on both levels, average-weekly deformation rate was higher when blasting occurred on the level above (Fig. 6). The comparison cannot be made for blasts closer than 30 m as there are no blasts from the level above that can ever occur when r is less than the sub-level interval height (30 m).

The data also provides clues about the relative importance of inclination angle vs. that of distance. The weekly deformation rates from all weeks during which blasting occurred when $r < 10$-m ($n = 9$) were aggregated and averaged. The same was done for all weeks in which blasting occurred when $\varphi > 60°$ ($n = 36$). Calculating the average-weekly deformation rates that occurred in each group provided the information shown in Table 5.

The results tend to indicate that deformation rates are higher when r is less than 10 m, which can only occur when production blasting is on the same level as the instrument,

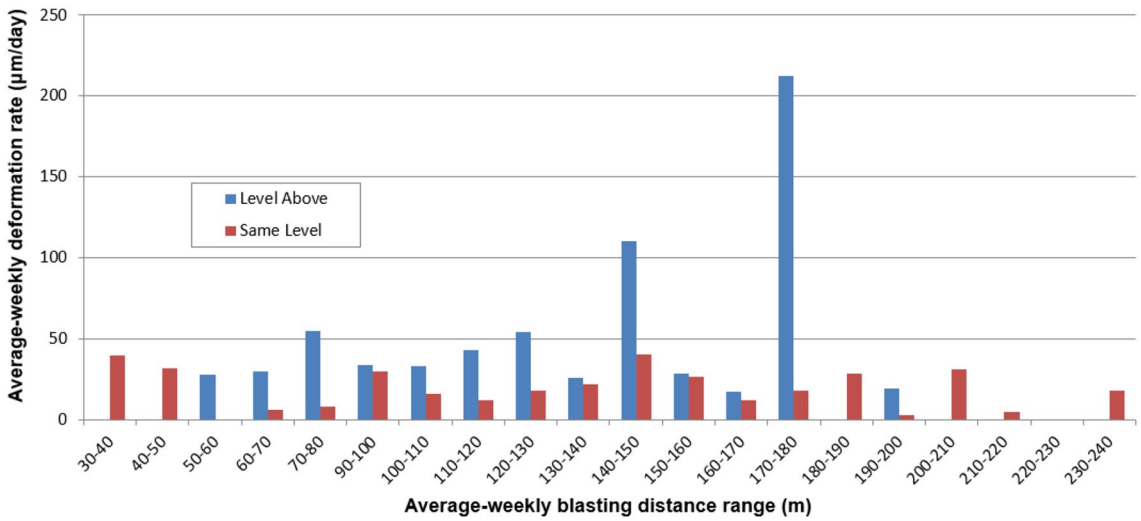

Fig. 6 Average-weekly deformation rates for production blasts occurring on levels above the instruments and on the same level as the instruments, divided into distance ranges

Table 4 Site specific RQD values and generalized RMR parameters for each bolt group, compared with average displacement of the collar anchors

Bolt #	Group ID	RQD min	RQD mean	RQD max	Generalized GSI	Average deformation (mm)
1–4	A	85	93	98	55–65	0
5–8	B	57	73	82	35–55	7
9–10	C	100[a]	100[a]	100[a]	65–75	0
11–14	A	59[a]	82	90	55–65	0
15–18	D	26	57	77	35–55	38
19–20	C	67	75	87	65–75	0

[a]Core disking present

Table 5 Average-weekly deformation rates caused by very-close ($r < 10$ m) production blasts compared to those with high inclination angles ($\varphi > 60°$)

Event descriptor	Sample size (n)	Average-weekly deformation rate (µm/day)
Blasts < 10 m away	9	98
Blasts > 60°	36	72

than when φ is greater than 60°, which can only occur when production is on the level above. Though this result seems to contradict Fig. 6, it is not necessarily the case and the results should be considered carefully. The sample size of blasts that occur closer than 10 m to the instrument is too small to draw strong conclusions, and the worst-case scenario of an inclination angle of 90° is not tested in this layout due to mine geometry. The crosscuts on the level above are offset in such a way that the theoretical maximum inclination angle in this mine plan is approximately 63°, though in practice angles up to 72° were calculated. Also, the great range of deformation rates experienced from this dataset make it such that the averages shown in Table 5 may not accurately represent the real case.

This data will be the beginning of an empirical database used to determine and predict mining-induced deformation in each location based on geotechnical parameters and the location of production blasting. Given that the most critical variables in use here are all relative to one another (relative positioning of production blasts compared to a location of interest, and the relative geotechnical parameters and stiffnesses of adjacent geologies), the techniques should be useful knowledge to other mining operations with similar conditions.

3.3 Deformation Rate

Deformation rate is of greater interest than deformation magnitude when considering the issues of stability and impending failure because high deformation on its own is

not necessarily cause for alarm, though increasing deformation rate is typically a sign of pending problems. To help ensure that the stress redistribution and rock-mass destabilization caused by production blasting was the cause of the increased deformation rates, only those instrument readings that occurred during weeks in which blasting occurred were considered, a total of 580 average-weekly deformation rate samples. Because there were so many low-rate values (normal deformation levels), a deformation-rate threshold was set at the 95th percentile level to focus further analysis onto the most important events. This threshold was 150 µm/day and was the lowest average-weekly deformation rate experienced by the top 5% (29 samples) of all average-weekly deformation rates.

Every average-weekly deformation rate value is calculated from all the readings that were recorded during that week for a single instrument, and each individual reading shows the impact of an individual production blast on an individual instrument. This allowed for back-analysis to determine exactly which production activities contributed to high deformation rates. Only instruments from groups B and D showed significant movement, recording a total of 1026 non-averaged deformation rate readings over their span of operation. Of these, only 44 readings (4.3%) were found to be above the previously-determined 150-µm/day threshold.

The 44 high-rate records yielded insight into the types of mining activities most likely to cause elevated deformation rates. At least one specific production blast could be identified as the causal activity for each occurrence of high deformation rate. This resulted in a total of 46 causal activities (two high-rate records had two causal activities attributed). From these, six categories of causal-activity-type emerged, as shown in Table 6, plus four unexplained high-deformation rates. These six causal-activity-types are described below and detail mine-induced deformation scenarios that occur during the mining process.

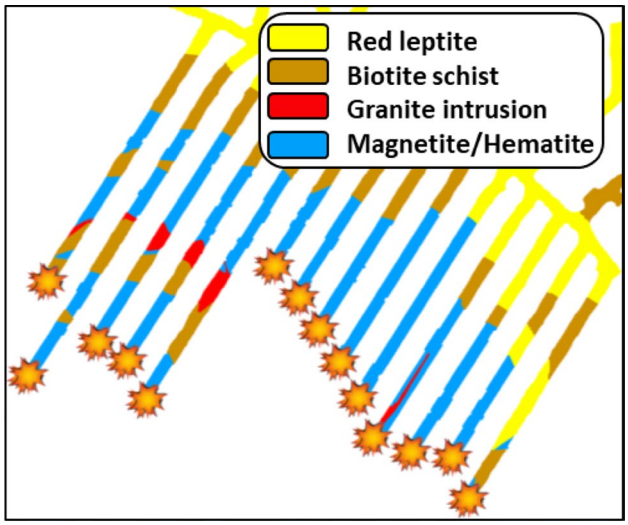

Fig. 7 Scenario 1, illustrating that opening blasts occur at the beginning of each crosscut where they create large disturbances in the stress field

3.3.1 Scenario 1

The first three blasts in each crosscut are located closer to one another (1.2 m instead of 3.5 m apart) and are all initiated at the same time to produce a large opening to initiate further caving (Fig. 7). This creates a large, sudden shift in the local stress fields. This shift impacts deformation rate a great distance away; it was 77-m distance between bolt 17 on level 962 and the opening blasts of crosscut 4781 on level 932. This type of event has a much greater impact on local stresses, and, therefore, deformation, than any of the other event types, i.e. it has impact from the greatest distance (similar to Larson and Lawson 2015). This scenario averaged a 240-µm/day deformation rate.

Table 6 Causal activity types and their frequencies of occurrence, as well as the average deformation rate resulting from the activities in each scenario and the percentage of high deformation rate events explained by each scenario type

Scenario #	Causal event	Count	Avg. def. rate (µm/day)	Percentage
1	Opening blasts of new crosscut	8	240	17.4
2	Blasting approaches and contacts the footwall	15	483	32.6
3	Blasting approaches and contacts an ore/biotite schist contact	8	410	17.4
4	Blasting approaches an instrument in the same crosscut	6	267	13.0
5	Blasting in neighboring crosscuts passes an instrument	3	190	6.5
6	Time-dependent deformation	2	206	4.4
	Uncategorized	4		8.7

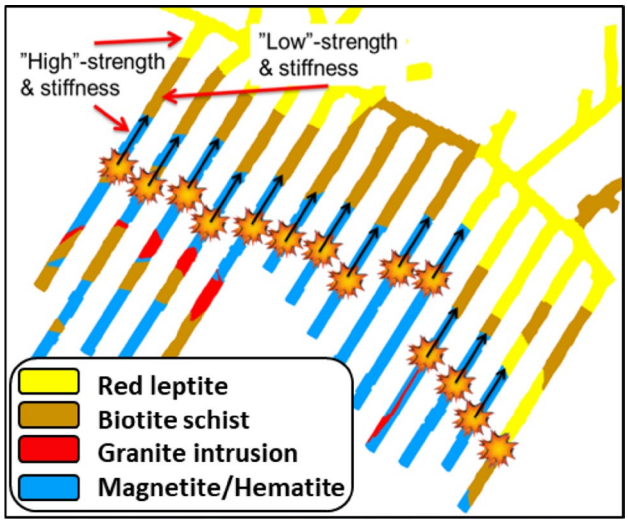

Fig. 8 Scenario 2, illustrating that production blasts proceed down each crosscut, approaching the footwall contact (movement indicated by arrows)

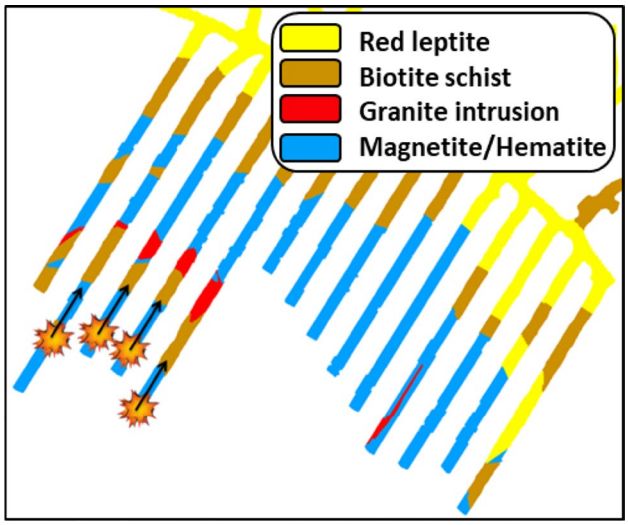

Fig. 9 Scenario 3, illustrating how production blasts proceed down the crosscuts approaching a biotite/granite intrusion within the orebody

3.3.2 Scenario 2

When production blasting proceeds down the crosscuts and nears the footwall contact between the stronger magnetite and the weaker biotite schist, the magnetite preferentially carries the stress of the area, since the less-stiff biotite can not. As blasting proceeds, the width of the magnetite decreases with each successive blast, reducing the cross-sectional area of the magnetite in plan view, as in Fig. 8. The magnetite thins and transfers additional stress onto the weaker biotite schist, causing an average of 483-μm/day in the schist. This behavior actually has many published precedents, though they come from longwall coal mining (Listak and Bauer 1989; Oyler et al. 1998; Thomas 2008; Qiu and Luo 2013; Gearhart et al. 2014). They are applicable since it is the relative stiffness of the geologic units, not the rock strength, that is the critical factor.

3.3.3 Scenario 3

This scenario is functionally similar to Scenario 2, except that instead of approaching the footwall, blasting approaches a biotite schist intrusion in the center of the orebody (Fig. 9). Occasionally an intrusion of high-stiffness granite accompanies the biotite schist intrusion. The schist and granite have a much smaller lateral extent than the actual footwall schist and leptite. It is hypothesized that as the blasting approaches the intrusion, the granite acts as a "pillar", and as the width of remaining ore between the cave and the granite gets thinner, increasing levels of stress are again redistributed to the schist in the intrusion. The magnitude of stress redistribution is likely lower than in Scenario 2 due to the relatively smaller cross section and lateral extent of the intrusion compared to that of the actual footwall, but the schist still experiences elevated deformation rates, averaging 410 μm/day.

3.3.4 Scenario 4

Deformation rates tend to increase as blasting gets very near to instrumentation installed on the same level as the blasting (Fig. 10). This increase is likely due to the very-low blast distances quickly altering the stress flow gradients in the immediate area, but also partly due to the blasting damage reducing the rock mass quality. Distances between the blast

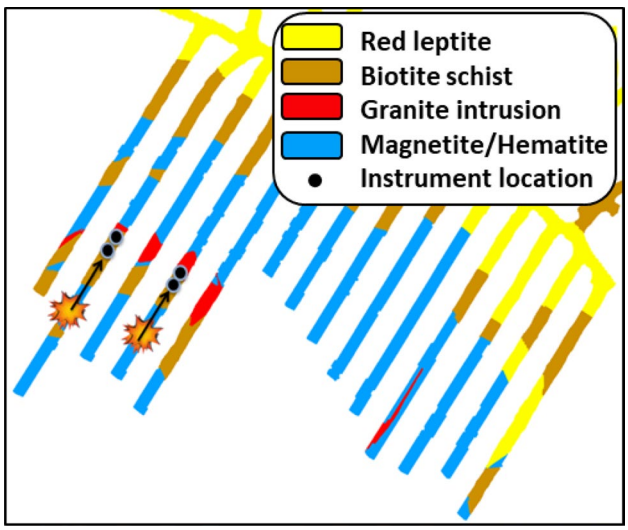

Fig. 10 Scenario 4, illustrating how blasts proceed down the crosscut approaching the instruments. Blasting distance becomes very low

location (as defined) and the instrumentation in this type of scenario can reach as little as 1 m, but can be up to 35 m. Naturally, closer blasts produce higher deformation rates, averaging 267 μm/day here.

3.3.5 Scenario 5

When blasting in nearby crosscuts approaches and passes an instrument, the instrument location experiences increased deformation. In this scenario, the rock is blasted on either side of the instrument, leaving the instrument in a pillar of rock. This pillar is required to support greater amounts of stress, leading to increased deformation rates (Fig. 11). The magnitude of deformation will be controlled by the geology in the pillar. The same redistribution occurs any time this scenario occurs, but greater magnitudes are experienced in the softer schist. Deformation rates averaged 190 μm/day for this scenario.

3.3.6 Scenario 6

High deformation rates can continue even after another blasting event corresponding to another scenario type occurs. In two instances, high deformation rates were experienced during the weeks immediately following another major event type. In these cases, time-dependent deformation continued as the rockmass attempted to equalize itself. The root cause of increased deformation rate in these cases belongs to other stress scenarios, but Scenario 6 events are listed separately as the blasting that caused the deformation occurred during the week prior. Partly because of this time delay, average deformation rates, while still considered to be high, are lower than most of the other scenarios (206 μm/day).

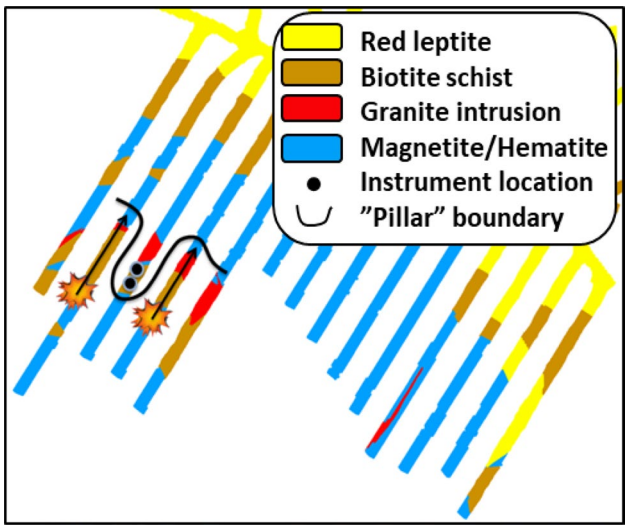

Fig. 11 Scenario 5, illustrating how production blasts proceed past on each side of the instruments move past forming a "pillar" of remaining rock

Of these stress scenarios, scenarios 2 and 3 are very similar to one another in that they are each examples of stress concentrations forming in a weaker material, directly impacted by the mine's production planning and scheduling. Together they account for half of all high-deformation-rate events, and as such, greater care should be paid to them in difficult areas of the mine. Their impact may be minimized by distributing their blasting over a longer time period, or otherwise altering the production scheduling to better control stress redistribution. If time-dependent deformation is critical, accelerating production through difficult areas might produce positive results. This technique is well-established in other mining methods.

4 Discussion

Many of the stress-scenarios identified can be seen when looking at the deformation results graphed in Figs. 4 and 5. Certain points are worth emphasizing. In the figures, the greatest amount of deformation always occurred, and at the fastest rate, when level 932 was being closed (averaging 710 μm/day between days 503–544). This event is part of Scenario 2, which is the most common of all scenarios. The data do not indicate if this high rate is specific to the conditions at the close of 932, but since the scenario is not based on specific rock conditions, but rather on the relative stiffness of adjacent rocks, it is likely that the same deformation pattern will occur at the close of future mining levels. In fact, the results for bolt 18 indicate that the close of level 962 has a similar pattern which implies the scenario is broadly applicable.

When compared with the average deformation rates for Scenarios 2 and 3, the rates that were experienced when blasting was completed either directly above the installed instrumentation on the level above, or very near to the instrumentation in the same crosscut, were both realitively low. These high-angle and very-near occurrences (Table 5) can be identified by locating those blasts in Figs. 3, 4 and 5 that have the lowest distances graphed for each mining level. The implication of this is that the hypothesized stress redistribution caused by Scenarios 2 and 3 is much more of an influence on deformation than simple production blast location or proximity.

The same patterns also indicate that the primary forces driving the deformation must be traveling laterally through the rock, or otherwise blasting directly above an instrument would have a much greater impact than is seen in this dataset. The most likely reason the forces are changing is that they are mining-induced. When considering only r and φ, current results indicate that nearby blasting may have a

greater effect than blasting directly above a location, though this conclusion would benefit from more data. Additional analysis will need to be completed to better understand how variations in φ and r affect deformation. Equivalence should also be determined between φ and r (i.e. at what inclination angle or blast distance are the impacts on deformation the same?). This should be part of the same analysis.

Another point of discussion is that much of this work is based on the idea that 150 μm/day is a significant static deformation rate. The rate analysis conducted here used a 5% statistical threshold, which is the source of, and corresponds with 150 μm/day in this dataset. The question presents itself, though: is 150 μm/day important to the mine? The threshold rate was chosen in this case based on simple statistical methods, but effort needs to be made to determine whether or not that rate of deformation is acceptable to the mine. 150 μm/day can be restated as approximately 1 cm per 67 days, or approximately 5.5 cm/year. Instrument 17, which experienced the greatest total deformation, recorded a total of around 5.5 cm deformation over 2 years of monitoring. Certainly this rate is not acceptable on a long-term basis, but as said previously, increases in deformation rate are much more important in identifying potential instability.

The question remains; is the chosen threshold rate significant to the mine? Only regular damage mapping in instrumented areas can allow deteriorating conditions to be linked directly to deformation rate. This will be done in another study soon to be initiated. Once "significant" damage is identified in the mine, then "significant" magnitudes and rates can be determined to help make future analysis more useful. For now, it can be said that there are particular "causal activities" which tend to be linked to instances of higher deformation rates. Since causal activities are production-blast based, the ability to schedule the blasting in a favorable manner allows the mine to "schedule" periods of higher deformation rate. This increases safety for the workers.

The geometric methods used here are relatively straightforward in that they simply measure and utilize the relative positioning of the production blasts with respect to instrument location to better understand mining-induced deformation changes. The variables included in relative positions are suitable for determining many position-based effects of blasting, but a great deal of potential exists to expand on these relationships. For instance, while an attempt has been made to include some aspects of geology or rock quality at the instrument location, and greater emphasis will be placed on this in future research, no attempt has been made at all to include conditions of the rock that is interposed between instrument and blast. 3D geologic modeling completed in future study areas will be combined with geotechnical domain models to better understand the conditions existing between the production blasts and the instrumentation. This will be required to produce a true deformation model. The presence of faults, fractured zones, and rock of variable stiffness can all impact the transfer of stress through an area to a great degree. Future research will include this to a much greater extent.

Initial benefits of this research, improved control of deformation, will likely come from better understanding the impact of stress scenarios. If the scenarios described here can be further refined and better supported, even just with additional empirical evidence, they could allow immediate improvements to the mine's production planning. Production could be scheduled in such a way that it would minimize the impact on sensitive areas of the mine, or at least do so in a controllable way. Further refinements could allow improvements in rock support, and overall safety. The biggest immediate benefit of this research is the knowledge of how deformation occurs at the closing of the level above. The safety of the mine can be immediately improved by limiting employee exposure in hazardous areas during and immediately after the production blasting that creates the most deformation-prone scenarios.

Given that similar deformation patterns are found on both levels 932 and 962, as well as in multiple locations around the individual levels, indicates that these deformation patterns are not exclusive to a specific location in the mine. Additionally, it implies that the forces driving the deformation must be larger-scale in nature rather than simple local events. These are likely not global-scale forces, as the deformation is not experienced everywhere and in all instrumentation. The conclusion is that they are likely orebody-scale forces that are working in conjunction with local geological and geotechnical factors that produce similar results in many places.

The fact that highly similar deformation patterns can be seen often in longwall coal mining (Listak and Bauer 1989; Oyler et al. 1998; Thomas 2008; Qiu and Luo 2013; Gearhart et al. 2014) again indicates that these patterns of stress redistribution exist in other operations, and even in other segments of the mining industry. These relationships are just beginning to be explored in the context of a sublevel caving operation, but there exists a high potential for knowledge improvement and the ability to predict and control deformation in these types of conditions, which are in no way exclusive to longwall mining, sublevel caving, or underground iron production. It indicates that the relationships being explored here have the potential to be of use in many segments of the mining industry.

The aim of future efforts is to design a model that allows for forecasting of deformation in sensitive areas of the mine well in advance based on pre-mining and development-mining data. It could be expanded to include impact on all areas of the entry, and not just the roof. The ability to better-predict deformation could reduce support requirements and costs,

both in labor and supplies, by allowing the installation of extra support only where needed, and in advance. Finally, the better understanding of stress scenarios could help to improve mine production scheduling, in turn helping to reduce production downtime due to rock-mechanics related problems. Follow-up research will begin soon which will include stress instrumentation to better answer questions relating to the driving factors of deformation in these conditions.

5 Conclusions

Mine production blasting redistributes stresses in the mine and causes direct degradation of the nearby rock mass. The damage and stress alterations both cause increased deformation magnitude and rate. The location of the blasts relative to the instrumentation (or a particular location) is an important variable influencing some of the relationships governing deformation.

Roof extensometer data and the mine's global coordinate system have been used to determine the relative positioning of instrumentation with respect to production blasting in an underground sublevel caving mine. The use of simple geometric relationships has been a useful tool for the analysis of this dataset. While the method is simple, it has helped create a better understanding about the impact of geometry, geology, and geotechnical parameters on deformation. In combination with previous work from other portions of the mining industry, it is seen that the relative stiffness of adjacent geologic units is of great importance in controlling the amount of deformation that is experienced in either of the units. The stiff unit tends to limit deformation in the softer unit until enough of the stiff unit has been removed during mining that the softer unit has no choice but to deform as it accepts a greater portion of the load.

The distance (r) and inclination angle (φ) between SMART cable bolts and production blasts were used as independent variables while assessing their contribution to the roof deformation and deformation rate experienced at the instrumented locations. The major results of this work with respect to geometry are:

- Elevated inclination angles result in greater roof deformation rates when blasting is compared between two different production levels. Those blasts occurring on levels above create greater deformation.
- Shorter distances create greater deformation than longer distances when blasting occurs on the same level as the instrumentation. That being said, when blasting is on levels above, aspects of inclination angle come into play.
- An analysis of deformation rate has been useful for identifying and developing the concept of "causal activities". The scheduling of production blasts can create stress conditions which increase the deformation rates in sensitive areas.
- Poor rock quality in the location of an instrument tends to increase the amount of deformation measured there.
- In this study, the re-distribution of mine stresses has a greater impact on deformation than does blasting damage proximity.

This work has identified six causal activity types that together account for 91% of the high-deformation-rate events experienced during the study period. Initial theories with respect to their creation and how they function within the changing stress state of the mine and its geology have been developed. This new information about which mining activities tend to increase deformation the most will allow the mine to better schedule production activities, giving it greater control over precisely when and where the deformation will occur. On a broader basis, the relationships between the relative stiffnesses of rock and how they affect deformation when exposed to stress increases will be used to help develop prediction tools for deformation. As they will be based on relative geotechnical values only, it is hoped that they will be applicable to many other sites beyond the mine itself.

While most of these results correspond greatly with common-sense expectations and with past research results, the true value here is not in identifying their existence in this mining case, but rather in beginning to understand how they interact with each other to drive deformation. Further work on this topic has the potential to lead to some very beneficial outcomes for the mine, and when expanded as a method, to other mining locations around the world.

Acknowledgements The authors would like to acknowledge LKAB for their assistance and data access during this project. Funding for the work has been partially provided by the European Commission 7th Framework Programme for the I^{2}Mine Project (Grant number 280855) and by the Center of Applied Mining and Metallurgy (CAMM) at Luleå University of Technology.

References

Atlas Copco (2007) Mining methods in underground mining, 2nd edn. Atlas Copco, Örebro

Basarir H (2013) Evaluation of field measurement results in Malmberget. Luleå

Bieniawski ZT (1992) A method revisited: coal pillar strength formula based on field investigations. In: Iannacchione AT, Mark C, Repsher RC et al (eds) Proceedings of the workshop on coal

pillar mechanics and design—IC9315. US Bureau of Mines, pp 158–165
Blanchowski J, Ellefmo S, Ludvigsen E (2011) Monitoring system for observations of rock mass deformations caused by sublevel caving mining system. Acta Geodyn Geomater 3:335–344
Brunton ID, Fraser SJ, Hodgkinson JH, Stewart PC (2010) Parameters influencing full scale sublevel caving material recovery at the Ridgeway gold mine. Int J Rock Mech Min Sci 47:647–656. https://doi.org/10.1016/j.ijrmms.2009.12.011
Capes GW, Doolan JP, Neindorf LB (2007) Stope design considerations using rock mass classification tools at the Xstrata Zinc George Fisher mine. In: Proceedings of the international workshop on rock mass classification in underground mining. Center for disease control
Chen B, Deng K, Fan H, Hao M (2013) Large-scale deformation monitoring in mining area by D-InSAR and 3D laser scanning technology integration. Int J Min Sci Technol 23:555–561. https://doi.org/10.1016/j.ijmst.2013.07.014
Colwell MG (2006) A study of the mechanics of coal mine rib deformation and rib support as a basis for engineering design. University of Queensland
Colwell M, Hill D, Frith R (2003) ALTS II—a longwall gateroad design methodology for Australian collieries. In: 1st Australasian ground control conference. University of New South Wales, pp 123–135
Coon RF, Merritt AH (1970) Predicting in situ modulus of deformation using rock quality indexes. In: Determination of the in situ modulus of deformation of rock—ASTM STP477. ASTM, Philidelphia, p 20
Dahl HD (1978) The state of the art in underground coal mine design. In: International symposium on stability in coal mining, Vancouver
Deere DU, Coon RF, Merritt AH (1996) Engineering classification of in-situ rock. Technical Report No. AFWL-TR-67-144. Urbana
Fernandez F, Watt G, Ooi J (2012) Strategic management for squeezing ground conditions at the Argyle Diamonds block cave project. Aust J Civ Eng 10:193–206. https://doi.org/10.7158/C12-002.2012.10.2
Franklin JA, Dusseault MB (1989) Rock engineering. McGraw-Hill, New York
Gearhart DF, Jones TH, Compton CS et al (2014) Ground response as a longwall advances into a backfilled recovery room under low cover. In: 33rd International conference on ground control in mining, Morgantown, pp 1–10
Henry E, Mayer C, Rott H (2004) Mapping mining-induced subsidence from space in a hard rock mine: example of SAR interferometry application at Kiruna mine. CIM Bull 97:1–5
Hidalgo KP, Nordlund E (2014) Deformation analysis in connection with bending and shear failure of a monitored stope in the Kristineberg mine in Sweden. Int J Min Miner Eng 5:181–201
Idris MA, Basarir H, Nordlund E, Wettainen T (2013) The probabilistic estimation of rock masses properties in Malmberget Mine, Sweden. Electron J Geotech Eng 18:269–287
Jin A, Sun H, Wu S, Gao Y (2017) Confirmation of the upside-down drop shape theory in gravity flow and development of a new empirical equation to calculate the shape. Int J Rock Mech Min Sci 92:91–98. https://doi.org/10.1016/j.ijrmms.2016.12.005
Jones TH (2016) Production-blast-induced crosscut performance: a comparison of three high-deformation bolt types. In: Nordlund E, Jones TH, Eitzenberger A (eds) 8th international conference on ground support in mining. Luleå University of Technology, Luleå, pp 1–11
Larson MK, Lawson HE (2015) Load transfer distance measurements at two mines in the western U.S. In: 34th international conference on ground control in mining. West Virginia University, Morgantown
Listak JM, Bauer ER (1989) Front abutment effects on supplemental support in predriven longwall equipment recovery rooms. In: The 30th U.S. symposium on rock mechanics (USRMS). American Rock Mechanics Association, Morgantown
Lupo JF (1996) Evaluation of deformations resulting from mass mining of an inclined orebody. Colorado School of Mines
Mark C (1987) Analysis of longwall pillar stability. Pennsylvania State University
Mark C, Chase FE (1997) Analysis of retreat mining pillar stability—IC 9446. Pittsburgh, Pennsylvania
Matthews KE, Hoek E, Wyllie DC, Stweart SBV (1980) Prediction of stable excavation spans for mining at depths below 1,000. Report 802–1571. CANMET
Mine Design Technologies (2018) SMART cable bolt. https://mdt.ca/products/instrumentation/smart-cable-bolt/. Accessed 12 Oct 2017
Nordlund E (2013) Deep hard rock mining and rock mechanics challenges. In: Potvin Y, Brady B (eds) Ground support 2013. Australian Center for Geomechanics, Perth, pp 39–56
Oyler D, Frith R, Dolinar D, Mark C (1998) International experience with longwall mining into pre-driven rooms. In: 17th international conference on ground control in mining. West Virginia University, Morgantown, p 10
Pakalnis RT (1986) Empirical stope design at the Ruttan Mine, Sherritt Gordon Mines Ltd. University of British Columbia
Qiu B, Luo Y (2013) Applications of subsurface subsidence theories to ground control in coal mines. In: 47th US rock mech symp
Rech WD, Watson DK (1994) Cave initiation and growth monitoring at the Henderson mine. In: SME annual meeting. Albuquerque, p 8
Salamon MDG, Wagner H (1985) Practical experiences in the design of coal pillars. In: 21st int. conf. saf. mines res. institutes, vol 21, pp 3–10
Struthers MA, Turner MH, McNabb K, Jenkins PA (2000) Rock mechanics design and practice for squeezing ground and high stress conditions at Perseverance mine. In: MassMin 2000. Australasian Institute of Mining and Metallurgy, Brisbane, Queensland, pp 755–764
Sundström R (2010) Utvärdering av Smart Cable för att se belastning på bergbultar. Luleå University of Technology
Swart AH, Handley MF (2005) The design of stable stope spans for shallow mining operations. J S Afr Inst Min Metall 105:12
Thomas R (2008) Recent developments in pre-driven recovery road design. In: 27th international conference on ground control in mining. West Virginia University, Morgantown, pp 197–205
Villegas T, Nordlund E, Dahner-Lindqvist C (2011) Hangingwall surface subsidence at the Kiirunavaara Mine. Eng Geol 121:10. https://doi.org/10.1016/j.enggeo.2011.04.010
Wagner H (1974) Determination of the complete load-deformation characteristics of coal pillars. In: Proc. 3rd ISRM congr, vol 2, pp 1076–1081
Wettainen T, Martinsson J (2014) Estimation of future ground vibration levels in Malmberget town due to mining-induced seismic activity. J S Afr Inst Min Metall 114:10
Woo K-S, Eberhardt E, Elmo D, Stead D (2013) Empirical investigation and characterization of surface subsidence related to block cave mining. Int J Rock Mech Min Sci 61:12. https://doi.org/10.1016/j.ijrmms.2013.01.015